Effect of elastohydrodynamic film thickness on a wear model for worm gears

K. J. Sharif, H. P. Evans, R. W. Snidle, D Barnett and I. M. Egorov

Proceedings of the Institution of Mechanical Engineers, Part J: Journal of Engineering Tribology 2006 220: 295
DOI: 10.1243/13506501JET122

Effect of elastohydrodynamic film thickness on a wear model for worm gears

K J Sharif[1], **H P Evans**[1]*, **R W Snidle**[1], **D Barnett**[2], and **I M Egorov**[3]
[1]Cardiff School of Engineering, Cardiff, UK
[2]Renold Gears, Holroyd Gear Works, Rochdale, UK
[3]Department of Machine Design, Mechanical Engineering Faculty, St Petersburg State Polytechnic University, St Petersburg, Russia

The manuscript was received on 27 July 2005 and was accepted after revision for publication on 28 October 2005.

DOI: 10.1243/13506501JET122

Abstract: Worm gears used for power transmission commonly consist of a steel worm running against a bronze or phosphor bronze worm wheel. The wheel teeth are usually manufactured using an 'oversize' hob so that the initial elastic contact between the teeth is in the form of an ellipse with lubricant entrainment predominantly in the major axis direction. As a result of this unfavourable contact geometry, the lubricant film generated between the worm and wheel teeth is relatively thin. The kinematic configuration is close to that of simple sliding as the velocity of the wheel tooth surface relative to the nominal contact point is very low in comparison with that of the worm. The combination of poor film forming, high sliding and a soft gear material (to avoid scuffing) leads to the continuous wear seen in these gears.

The article presents results obtained using a model for the prediction of wear for this configuration based on the well-known Archard wear law extended to take the variation of pressure and film thickness over the contact area into account in determining the wear rate. The pressure and film thickness distributions are obtained from elastohydrodynamic lubrication (EHL) modelling of the contact over the meshing cycle. Wear patterns are presented corresponding to different film thickness sensitivities in the wear formula, and these predictions, together with the calculated increase in backlash due to wear, give a basis for calibrating the model against experimental wear tests.

Keywords: worm gears, wear model, elastohydrodynamic lubrication (EHL)

1 INTRODUCTION

Worm gears are possibly unique among gear power transmission systems in that the geometry of the load bearing areas of the teeth is changed continuously by wear processes during the lifetime of the gear pair. The configuration adopted for the current study is the most common one for power transmission applications: a steel worm component meshing with a phosphor bronze gear wheel. Gears of this form are usually manufactured with an 'oversize' hob that gives a contact that occurs at a point rather than a line under zero load, so as to obtain benefits in hydrodynamic lubrication and to avoid contact areas that reach the physical edges of the meshing components. The kinematic action of worm gears means that the wheel component is almost stationary relative to the contact point, and the formation of an elastohydrodynamic lubrication (EHL) film is therefore mainly due to the simple sliding motion of the worm. Consequently, the wheel component is subject to wear because of the sliding action of the worm over its surface. The steel worm also experiences wear but it is found, in practice, that this occurs at a much lower rate than that found in the wheel. The bronze teeth of the wheel are able to sustain this aggressive lubrication regime without scuffing, and their steady loss of material due to wear is recognized as an inevitable feature of these gears. Indeed, the extent to which

*Corresponding author: School of Engineering, Cardiff University, Queen's Buildings, The Parade, Newport Road, Cardiff, CF24 3AA, UK. email: evanshp@cf.ac.uk

material has been lost is assessed during maintenance inspections by measuring the increase in backlash, and this change is monitored until its extent indicates that wheel tooth strength is compromised.

During operation of the gears, there is an initial period of relatively rapid wear that is usually referred to as *bedding in*. During this phase, the actual contact area of the teeth under load increases thereby reducing the (average) contact stress levels. After bedding in has occurred, the gear pair tends to wear at a lower, reasonably steady, rate for the remainder of its life cycle. This steady wear rate can be influenced by a number of operating factors and effectively determines the lifetime of the gear mesh.

The gear surfaces are able to sustain the high levels of sliding to which they are subjected because of the EHL mechanism that can generate a lubricant film to separate the surfaces. This is the lubrication mechanism that protects the contacting surfaces of most gear pairs, but film forming in worm gears is far from optimal. The contact area over which the load is carried tends to be a long thin ellipse, which for some designs can be distorted into a banana shape because of the enveloping nature of the surfaces. Such a configuration could yield relatively thick lubricant films, if lubricant entrainment was in the direction of the minor axis, i.e. across the contact area. Unfortunately, this is not the case as the sweeping action of the worm ensures that entrainment is effectively along the major axis of the contact ellipse. The authors have previously examined the film forming capability of a large number of worm gear designs [**1**, **2**] based on a full EHL analysis (including thermal effects), and this study identified locations of particularly severe film thinning within the contact area because of the unfavourable kinematic action of the gears.

This article presents the means by which the EHL film forming analysis has been incorporated into a wear model of the tooth contact pair. The wear rate is determined at each point on the wheel tooth surface taking the EHL pressure and film thickness into account in a generalized wear formula. Integration of the wear rate over the meshing cycle then determines the tooth wear per wheel rotation. The wear is not uniform and modification of the effective contact area takes place. This effect of wear on wheel tooth geometry is taken into account in the model by recalculating the EHL film and pressure distributions at the end of a series of wear stages and incorporating the calculated change in wheel tooth shape into the subsequent calculations.

2 THEORY

The shape of the surfaces of the teeth of the gears is obtained from a 'cut and mesh' worm gear contact model developed by Fish and Munro [**3**]. This analysis considers a series of positions of the worm gear and for each worm position, the wheel is brought into contact with it in a geometric model. This process establishes the point of contact under zero load and the direction of the common normal at the contact point. The position of a series of points on the surface of the worm and the wheel tooth is obtained and these are fitted with a high-order polynomial of the tangent plane co-ordinates. The polynomials are taken to describe the initial shapes of the contacting surfaces for the subsequent EHL analysis.

Figure 1 presents a schematic view of the contact area between the worm and wheel tooth. The area of potential contact is delimited by arc AB that is the outer radius of the worm tooth surface, wheel tooth facewidth boundaries AC and BF, and the outer radius of the wheel tooth, CF. Arc DE within boundary CF corresponds to the recess or 'throat' present in the central part of the wheel tooth that accommodates the core diameter of the worm. The lubricant entrainment vectors (mean velocity of the two surfaces relative to their instantaneous contact) are indicated schematically by the curved arrows. Because of the dominance of the worm motion relative to the contact, entrainment is essentially along circular arcs centred on the worm axis. By use of an 'oversize' hob and careful adjustment of its offset and axis of inclination during manufacture of the wheel it is possible to achieve an elastic contact between the teeth of both required length and position within the potential contact area. This approach is used by manufacturers to avoid damaging edge contact and also, by placing the contact towards the exit side of the wheel tooth, aims to give an adequate converging inlet sweep to the contact for the generation of an EHL film. A typical contact area is shown schematically in Fig. 1.

The model of EHL in a worm gear contact presented in this paper is based on the Reynolds equation, which quantifies hydrodynamic action, together with an analysis of local elastic deformation

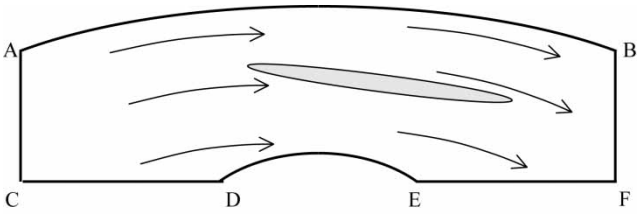

Fig. 1 Schematic diagram of the worm/wheel tooth contact area delimited by worm outer radius AB, wheel face boundaries AC and BF, wheel outer radius CF, and throat recess DE

arising from lubricant pressure. The kinematic conditions in worm gears are such that the entraining and sliding velocities vary both in magnitude and direction over the contact region. These effects are significant in the way they influence film generation and are therefore taken into account. A further important effect that must be included is that of non-Newtonian effects at high rates of shear arising from sliding within the contact. The formulation of a simultaneous numerical solution to the Reynolds and elasticity equations under these conditions is as follows. The authors have shown elsewhere [**1**, **4**] that it is necessary to formulate the lubricant flow behaviour in the local sliding and non-sliding directions, and this leads to the Reynolds equation of the form

$$\begin{aligned}&\frac{\partial}{\partial x}\left\{\left(D\cos^2\beta + C\sin^2\beta\right)\frac{\partial p}{\partial x}\right\}\\&\quad+\frac{\partial}{\partial y}\left\{\left(D\sin^2\beta + C\cos^2\beta\right)\frac{\partial p}{\partial y}\right\}\\&\quad+\frac{\partial}{\partial x}\left\{(D-C)\cos\beta\sin\beta\frac{\partial p}{\partial y}\right\}\\&\quad+\frac{\partial}{\partial y}\left\{(D-C)\cos\beta\sin\beta\frac{\partial p}{\partial x}\right\}\\&\quad=\frac{\partial}{\partial x}\left(\rho\hat{U}h\right)+\frac{\partial}{\partial y}\left(\rho\hat{V}h\right)\end{aligned}\tag{1}$$

Axes x and y are the principal axes of relative curvature in the tangent plane at the contact point. Parameters D and C are the flow factors in the sliding and non-sliding directions [**1**, **4**], and β is the angle between the local sliding direction and the x-axis. The other equation to be solved in the EHL system is the surface deflection equation. This is formulated in the differential form pioneered by Holmes *et al.* [**5**]

$$\begin{aligned}\frac{\partial^2 h(x_i,y_j)}{\partial x^2}+\frac{\partial^2 h(x_i,y_j)}{\partial y^2}&=\frac{\partial^2\phi}{\partial x^2}+\frac{\partial^2\phi}{\partial y^2}\\&\quad+\frac{2}{\pi E'}\sum_{\text{all }k,l} f_{k-i,l-j}\,p_{k,l}\end{aligned}\tag{2}$$

This formulation has the advantage that the pressure influence coefficients $f_{i,j}$ decay rapidly as the indices i and j increase from zero, and this allows the equations effectively to be solved simultaneously in the computing algorithm. The means by which these equations are solved is described in detail in references [**1**, **2**, **5**].

The wear rate is determined using the well-known Archard wear formula [**6**, **7**] which is adapted to take the variation of pressure and film thickness into account in the form

$$\text{Wear rate} = \frac{K}{H}pu_{\text{s}}\left(\frac{R_{\text{a}}}{h}\right)^n\tag{3}$$

Incorporating the local pressure in this way was used by Medina and Olver [**8**] in a study of spline contacts. The local sliding speed, u_{s}, takes on the role of sliding distance in the Archard wear formula when expressed in terms of wear rate (m/s) in this way. Modelling of wear in a lubricated situation is clearly dependent on the level of film thickness, and in equation (3), this is normalized to the surface roughness of the worm component. The sensitivity of the wear rate to film thickness is controlled by the power parameter n, which is regarded as disposable in the current study. In the overall empirical wear calculation included in relevant standards for worm gears [**9**], this power is specified as 2.24 which gives a wear rate when $h/R_{\text{a}} = 0.2$ of some 40 times that when h/R_{a} is unity.

Solutions to the previous equations are obtained at a sequence of meshing positions over the meshing cycle. The results for one such calculation with the 'as manufactured' geometry are given in Fig. 2 and are presented in terms of the tangent plane axes Oxy. The figure shows the contours of pressure and lubricant film thickness obtained by solving equations (1) and (2). Also shown is the instantaneous wear rate obtained by applying equation (3) to the solution for p and h. The contacts between worm gear teeth are heavily loaded in EHL terms [**2**]. This can be seen in Fig. 2 where the 50 MPa pressure contour is contained within the 1 μm film thickness

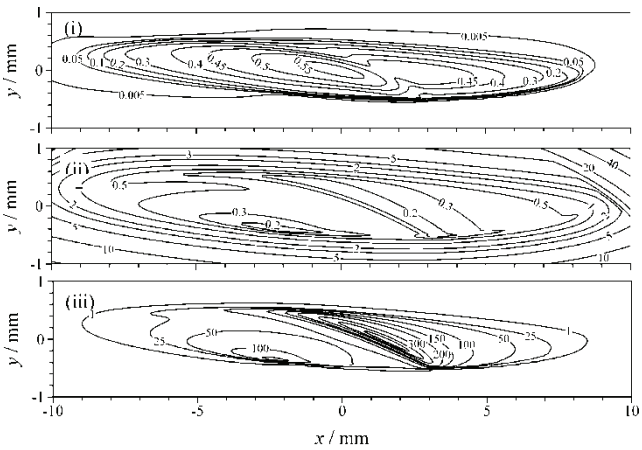

Fig. 2 Contours of (i) pressure/GPa, (ii) film thickness/μm, and (iii) calculated wear rate/nm s^{-1} obtained from an EHL solution at one point in the meshing cycle of a worm gear. Note that the y-axis is scaled by a factor of two to aid clarity

contour showing that there is very little pressure generation outside the corresponding dry contact area, which is contained within this 1 μm contour. The aspect ratio of the contact is about 15:1 and this has been distorted in the figure by a factor of two for clarity. The lubricant specified for the analysis is Mobil SHC632 gear oil used in experimental wear studies associated with this research. Its absolute viscosity at 60 °C is taken as $\eta = 0.093$ Pa and its pressure viscosity coefficient is $\alpha = 14.2$ GPa^{-1}. The central film thickness value is about 0.45 μm, and there are two regions of particularly thin film where values as low as 0.15 μm occur. These are the well-known side restrictions that appear in EHL oil films for elliptical contacts. In this case they are distorted by the sweeping entrainment velocity pattern [**2**] into the two thin film areas indicated in Fig. 2(ii). The rapid increase in film thickness seen in the top right corner of Fig. 2(ii) occurs at the outer radius of the worm component that is specified as a relieving radius of 40 mm.

When the contact occurs near the root of the wheel tooth its behaviour is essentially Hertzian and the area of dry contact can be established from a semi-infinite body analysis, as is inherent in the EHL solution scheme referred to above. As the contact moves towards the tip of the wheel tooth, however, the area of contact becomes longer and narrower, in practice, than that predicted on the basis of a semi-infinite body elastic analysis. This is due to the fact that tooth bending flexure under load influences the stiffness of the tooth in a non-uniform way with the tooth being stiffest at its centre and least stiff at the limits of its face width. A correction to the geometry is therefore introduced to ensure that the semi-infinite body treatment of elastic deflection embedded in the EHL analysis takes due account of this effect. This correction is applied in the form of a curvature change in the axial direction of the tooth, which is adjusted for each mesh position so as to obtain dry contact areas that coincide with those calculated on the basis of the tooth stiffness ideas described in references [**3**, **10**, **11**].

During the meshing cycle, the calculated wear pattern changes continuously and the area of high wear sweeps across the wheel tooth from its tip to its root (assuming that the worm is driving the wheel). Figure 3 shows the calculated wear rates obtained from EHL analysis as described earlier at six distinct contact positions over the meshing cycle. In Fig. 2, the wear rate contours are depicted in the tangent plane axes. These axes are different for each contact position considered. In Fig. 3, the calculated wear rates are presented in a projection plane perpendicular to the wheel axis as illustrated schematically in Fig. 1 and described earlier. In this and similar figures, the *xy* plane is perpendicular to the worm rotational axis. The *y* axis passes through the rotational axes of both worm and wheel, and is perpendicular to both. To determine the material removal for the whole tooth during a complete meshing cycle, the wear rate patterns illustrated in Fig. 3 are integrated over the meshing cycle by a process of interpolation and summation described in reference [**12**]. For this calculation the worm is considered at a series of equally spaced rotational positions which for a steady rotational speed are equally spaced in time. EHL calculations are carried out for each of these positions and the wear rate established from equation (3) as described earlier and illustrated in Fig. 3. The time integration required is carried out over 10 timesteps between each of the mesh positions for which an EHL analysis is undertaken. The wear at each of these timesteps is obtained by interpolating between successive wear rate calculations. The integration is thus from the beginning to the end of the meshing cycle and a typical result is shown in Fig. 4 where the contours plotted are those of the depth of material removed per meshing cycle, δ.

The amount of material removed during a single meshing cycle, in practice, is clearly very small and depends on the wear coefficient, *K*. For this study, the (dimensionless) value of *K* was taken as

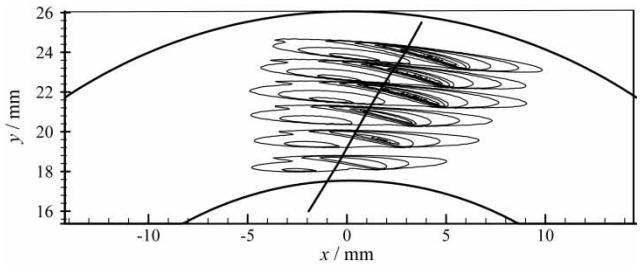

Fig. 3 Contours of wear rate calculated at a series of meshing positions on the wheel tooth surface. For each meshing position the contours shown are 25, 50, 100, 200, 250, 375, and 500 nms^{-1}. Solid curve indicates path of nominal contact point (under unloaded conditions) over the meshing cycle

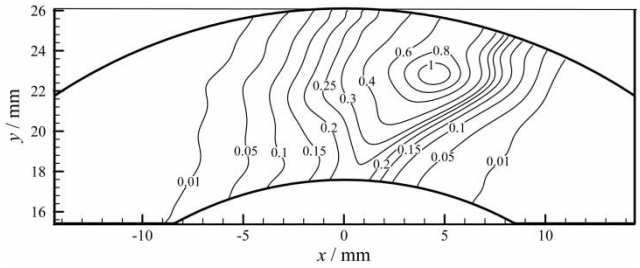

Fig. 4 Contours of δ/nm showing calculated wheel tooth wear over a single meshing cycle

2.5×10^{-8}, H for the wheel tooth was taken as 1 GPa, and the R_a value used was 0.5 μm. For the case considered the maximum wear depth in one meshing cycle is then 1.1 nm. Until such time as the accumulated wear from one meshing cycle to the next has made a significant change to the shape of the contacting surfaces, the amount of material removed during each successive meshing cycle will be the same and will be distributed over the tooth surface in the same way. Clearly this process cannot continue indefinitely as the tooth shape will gradually change with running time, and the way in which the pressure and film thickness are generated will also change. It is thus necessary to introduce the concept of a wear time step. This is the time, ΔT, for which the underlying geometrical shape is not significantly changed, and the wear rate per meshing cycle can be assumed to be unchanged. The relationship between the wear step time and real time is linear as the wear coefficient is an unknown, constant quantity that needs to be determined experimentally. It is thus possible to scale the data so that the maximum wear depth is a particular amount, say Δw. The wear step will then correspond to the real time in which a maximum of Δw is removed from the wheel by the wear process. For this article we take ΔT such that $\Delta w = 8.5$ μm. This corresponds to 7500 meshing cycles for the parameter values adopted. The worm rotational speed is 1200 r.p.m. and the gear ratio is 30 so that these meshing cycles occur in approximately 3 h.

Figure 4 shows that the wear rate is highest near the root of the wheel tooth. This is because the sliding speed, which is proportional to the radial distance from the worm's axis of rotation, is greatest at the outer part of the worm flank that makes contact with the root of the wheel tooth. A further factor that affects the wear is the shape of the elastic contact that becomes longer and narrower as the contact progresses towards the tip of the worm. This leads to higher pressures being generated in the contact together with thinner oil films as the shape of the contact becomes progressively elongated [**2**]. All these effects: higher sliding, higher pressure, and thinner films, lead to higher wear rates predicted by equation (3) and this explains the wear rate distribution seen in Fig. 4. To complete the cycle of modelling of the wear process, the material removal taking place in the wear stage is fed back into the calculation as a change to the underlying (undeformed) geometry, and the various calculation steps are then repeated on the basis of this new geometry.

The wear model thus consists of the following steps.

1. Determine the initial geometry of worm and wheel, and position of the contact points over the meshing cycle.
2. Carry out an EHL analysis at a sequence of mesh positions equally spaced in time during the meshing cycle. Determine the instantaneous wear rate for each point on the wheel tooth using equation (3).
3. Calculate the amount of material removed at each point on the wheel tooth during a single meshing cycle by integration in time. Scale these data by the number of meshing cycles occurring during the wear step to calculate the material removed over the tooth surface during the step.
4. Modify the undeformed geometry of the wheel tooth to take account of material removal. This completes the wear step.
5. Repeat from step 2 to determine the wear over the next wear cycle.

4 RESULTS

Sharif *et al.* [**12**] have considered a range of wear steps ΔT corresponding to Δw values of up to 20 μm. If the value of Δw is too large (greater than 16 μm for the case considered) the wear modelling process as described earlier becomes unstable. This instability is caused by an excessive change in geometry causing large changes in the EHL solutions obtained and thus in the wear rate calculated. Provided that Δw is below this threshold the modelling process is stable. By using a range of constant wear steps ΔT it is also shown in [**12**] that the calculated wear after several wear stages is independent of wear step size with the only significant differences being seen at the start of the process. This conclusion naturally leads to the less computationally demanding approach of determining the wear stage length in terms of the maximum material removal. Figure 5 compares the maximum wear rate calculated using (i) fixed wear stages ΔT corresponding to an initial maximum material removal depth of 8.5 μm, (ii) wear stages of duration $\Delta T/2$, and (iii) wear stages with a fixed value of Δw, $\Delta w = 4$ μm. As the intensity of the localization of the peak wear rate reduces during the initial wear stages, the constant Δw approach leads to increasingly large wear steps in terms of the wear time that they represent. Figure 5 shows that the processes are the same as far as the maximum calculated wear rate is concerned, which is a sensitive parameter in making this comparison. Figure 6 shows a comparison between the wear rate calculated at time $5\Delta T$ using these three approaches. (In this and similar figures, the wear rate is expressed in terms of the material removed in time ΔT). Figure 7 shows the same comparison for the total accumulated wear at time $6\Delta T$ in the wear process. Both figures demonstrate the equivalence of the

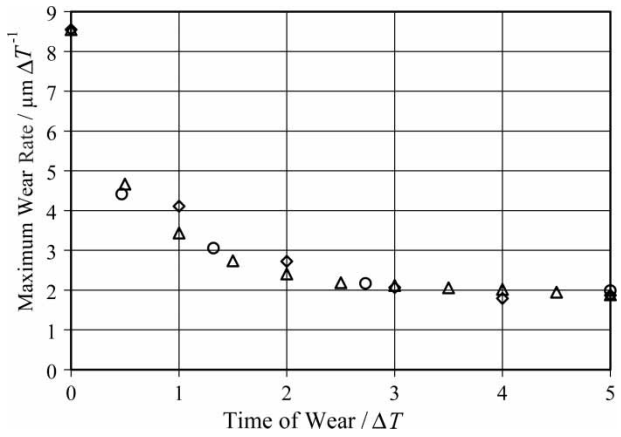

Fig. 5 Variation of maximum wear rate over the meshing cycle as calculated using different wear stage times. ◇: wear time ΔT, △: wear time $\Delta T/2$, ○: maximum wear $\Delta w = 4$ μm

two approaches, and consequently the constant Δw method is adopted as it is less computationally demanding for general use.

As the calculated wear process continues the area of the wheel tooth surface over which the load is carried (in the sense of high pressures and thin oil films) increases, and the contact area at any meshing position becomes longer and thinner. As a result, the contacts that were initially confined to approximately the middle third of the available tooth contact area as shown in Fig. 3, spread until they reach one or more of the boundaries of the available contact area illustrated in Fig. 1. This causes numerical difficulties in the EHL calculation due to the contact running off the edge of the available wheel tooth. To deal with these difficulties, a process of defining the edges of the tooth components with relieving radii has been adopted. Figure 8 shows the result of an EHL calculation for this situation where the contact has reached and crossed boundary AB in Fig. 1. The worm tip is defined by a relieving radius that is chosen so that the pressure generated beyond the boundary AB is trivial in comparison with the values obtained within the tooth contact. For the case presented in Fig. 8 this relieving radius is 40 mm.

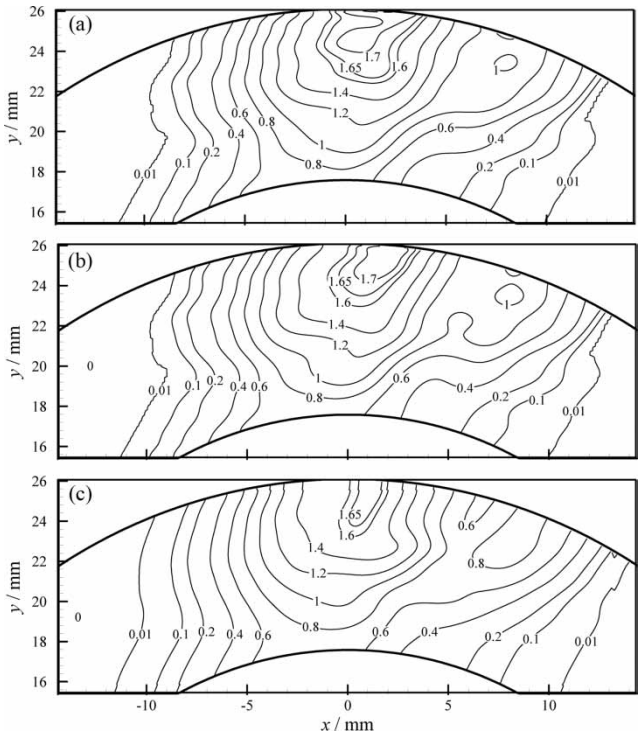

Fig. 6 Wear rate/μm ΔT^{-1} calculated after wear time $5\Delta T$ (a) using wear step $\Delta T/2$, (b) using wear step ΔT, (c) using fixed maximum wear steps $\Delta w = 4$ μm

If a smaller relieving radius is chosen then the results tend to produce a pressure concentration on the boundary AB together with direct contact between the surfaces. This is because the entrainment mechanism is weak along that edge which essentially corresponds to an entrainment streamline [2]. This is illustrated in Fig. 9, which was obtained with a sharper relieving radius of 5 mm. Contact occurs along the boundary at the arrowed position in Fig. 9(ii), and a corresponding pressure concentration develops inboard of this position as arrowed in Fig. 9(i). It may be noted that the EHL solver used is capable of dealing with mixed lubrication conditions where $h = 0$ at some points within the computing area [**5**, **13**], but a consequence of predicted contact is that the wear model of equation (3) generates an infinite wear rate under these circumstances. (The wear rate calculation in Fig. 9(iii) has been limited at the contact points to that which would occur at a film thickness of 1 nm according to equation (3).) Both the factors that typify the edge of the contact (high pressure and low film thickness) lead to high wear rates and conditions in this area are taken to change rapidly with localized wear relieving the pressure generated within the wear step. If this process is to be modelled in detail then the wear stages become extremely short in time, which defeats the object of the model. Numerical experiments in these circumstances indicate that the wear associated with the edge concentration is limited to the location of the edge and does not make a significant contribution to the overall solution. The process of defining the edge with a relieving radius carries with it the tacit assumption that wear at the very edge of the contact will be sufficiently rapid to relieve the stress concentration that will develop there if the edge is defined by a sharp change of slope such as a chamfer. Figure 10 shows

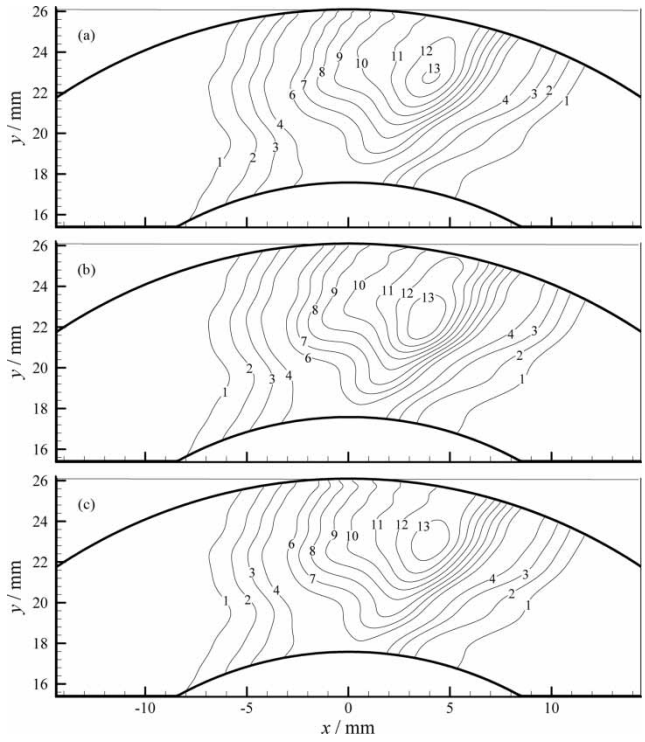

Fig. 7 Accumulated wear /μm after wear time $6\Delta T$ (a) using wear step $\Delta T/2$, (b) using wear step ΔT, (c) using fixed maximum wear steps $\Delta w = 4$ μm

the pressure, film thickness, and wear rate contours obtained without including the edge effects in the calculation.

Using these numerical techniques, it is possible to model the situation where the contacts spread over the whole surface of the wheel tooth. Figure 11 shows the total accumulated wear for the test case considered where the film thickness power is taken as $n = 2.24$. This value of n is used for all the results presented in this article unless otherwise specified. Figure 11(i) shows the case where the edge contacts are incorporated as described earlier. The total amount of material removed is 2.18 mm^3, and the maximum wear depth is 27.8 μm. Figure 11(ii) shows the corresponding result without considering the edge contacts. This comparison shows that the effect of incorporating the edge is to increase wear, not at the edges of the contact but in the middle. This is because taking the edge into account increases the load carried in the middle of the tooth. The wear at the edge is seen not to be different between the two cases on the scale of the maximum wear occurring on the tooth surface.

Figures of total accumulated wear allow comparison between models where the effect of film thickness on wear rate has been systematically varied. Three values of the parameter n controlling the influence of film thickness on wear have been adopted. The value $n = 2.24$ is the power included in the engineering standard [**9**] for worm gears, and the other values used are $n = 1$ and $n = 0$. (For the case $n = 0$, the wear rate depends only on the pressure, and the film thickness has no influence.) Figure 12 compares the total accumulated wear obtained with these three models. The basis for the comparison is the same total amount of material removed in the wear model which is 2.18 mm^3 as in Fig. 11. This comparison shows that when the film thickness is influential in determining wear, then wear is more prevalent towards the centre of the tooth. This view is reinforced by the comparison of the corresponding calculated wear rates at the time that 2.18 mm^3 of material has been removed as shown in Fig. 13.

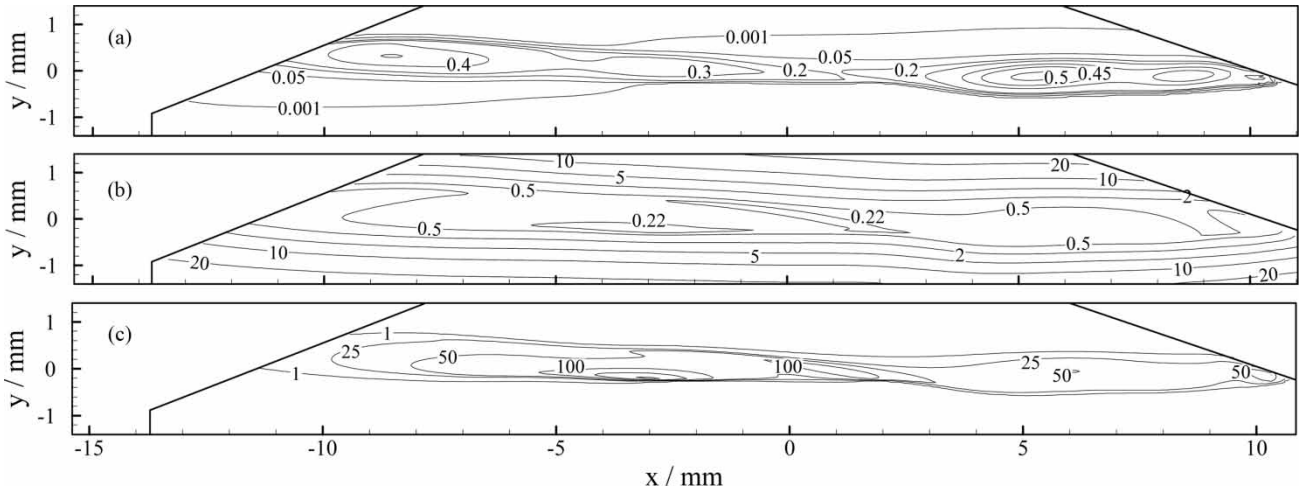

Fig. 8 Contours of (a) pressure/GPa, (b) film thickness/μm, and (c) calculated wear rate/nms^{-1} obtained from an EHL solution at wear time 6.7 ΔT at the meshing position considered in Fig. 2 with boundaries defined by a relieving radus (40 mm)

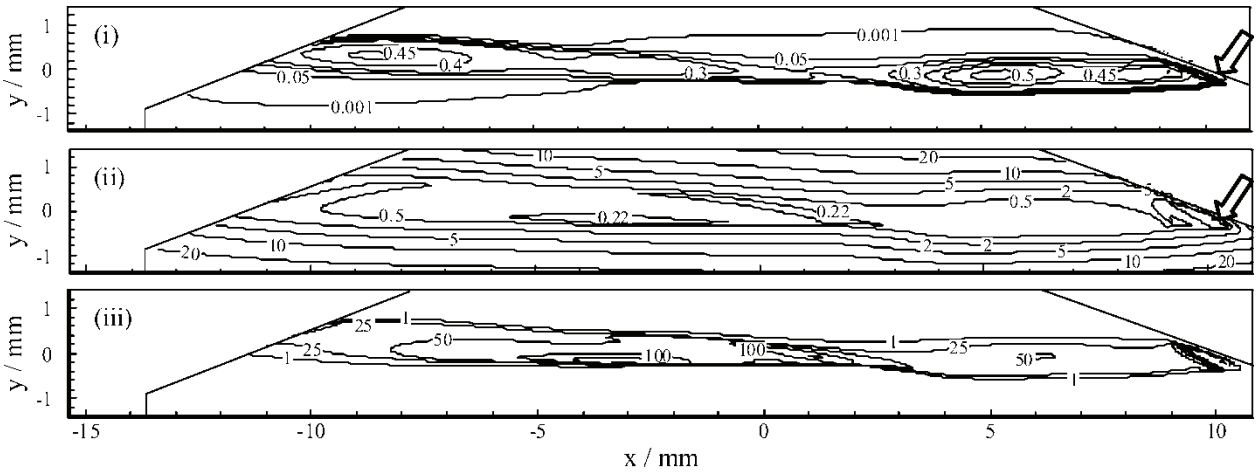

Fig. 9 Contours of (a) pressure/GPa, (b) film thickness/μm, and (c) calculated wear rate/nms^{-1} obtained from an EHL solution at wear time 6.7 ΔT at the meshing position considered in Fig. 2 with boundaries defined by a sharp relieving radius of 5 mm. Arrows indicate position of contact and associated pressure spike

In comparing the wear rates shown in Fig. 13 it appears that the case of Fig. 13(i) has lower wear rates. This is because low film thicknesses do not increase the wear rate in this case above that which corresponds to the pressure, and since each case carries the same load the pressures are of similar order between the cases shown. The tendency for film thickness dependence to concentrate wear in the centre of the tooth area is apparent from these wear rate comparisons. Figure 14 shows sections taken parallel to the x-axis for the accumulated wear surfaces of Fig. 12. These sections emphasise the differences in the accumulated wear patterns, and information of this sort can be compared to experimental measurements of the wear profile to establish the appropriate level of the film thickness power, n, in the wear formula.

To gauge the effect of wear on the EHL calculations, Figs 15 and 16 compare the pressures and film thicknesses obtained at a particular mesh position when the same amount of material has been removed with each of the three n values adopted. Figure 15 compares the pressure distributions. For the case with $n = 0$, the pressure developed tends towards a uniform distribution across the tooth. The pressure distribution for the case with $n = 2.24$ shows two centres of high pressure in the inlet and exit part of the contact with much lower pressures in the central part where the film thickness is particularly low. The case with $n = 1$ is intermediate

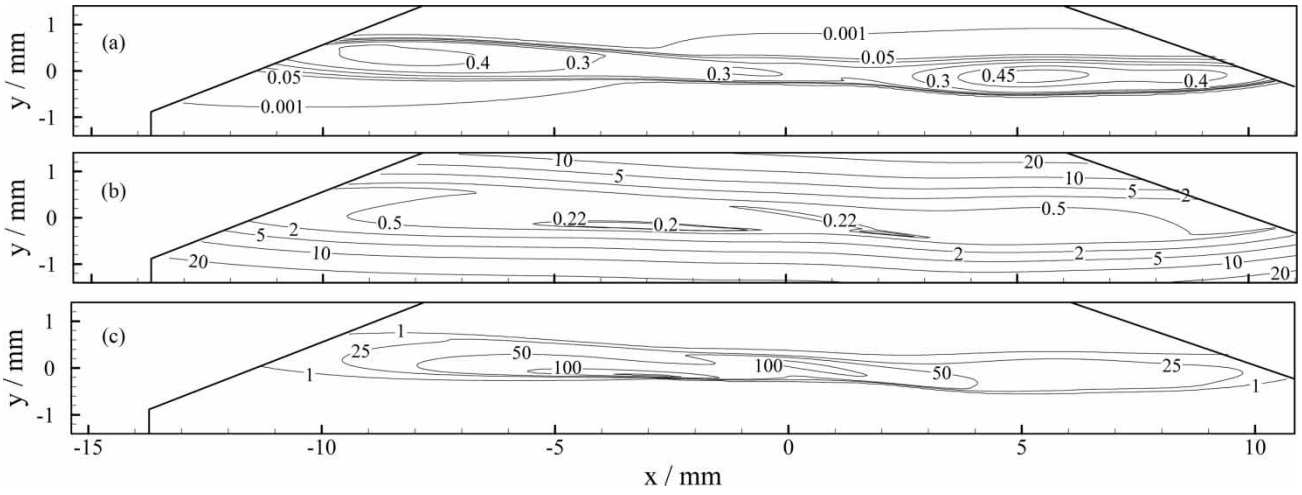

Fig. 10 Contours of (a) pressure/GPa, (b) film thickness/μm, and (c) calculated wear rate/nms^{-1} obtained from an EHL solution at wear time 6.7 ΔT at the meshing position considered in Fig. 2 with no change of curvature at boundaries

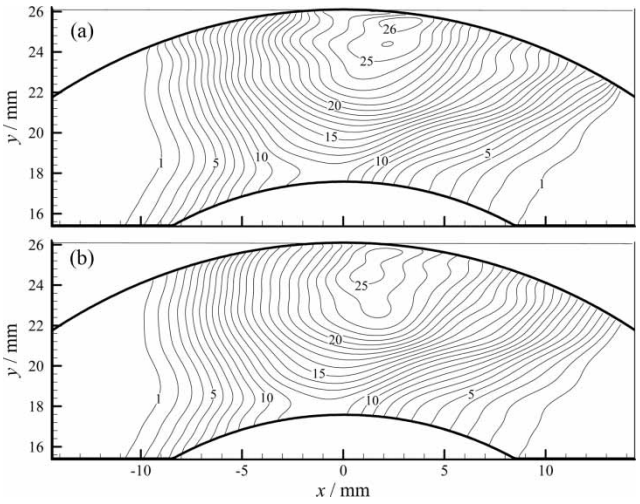

Fig. 11 Accumulated wear/μm when total material removed is 2.2 mm^3 (a) with boundaries defined by relieving radius of 40 mm, (b) where there is no change in curvature at the boundaries

with two centres of high pressure (but lower than seen in Fig. 15(i)) and a reduced pressure saddle area towards the middle of the contact. The film thickness distributions illustrated in Fig. 16 are very similar, particularly so in the cases of $n = 1$ and $n = 0$. For the case with $n = 2.24$, the interaction between thin film conditions and high wear rates has modified the thin film pattern. Material is being removed relatively rapidly in the location of the thinnest films and this remains the case until the pressure falls in that area as a result of the material removed. This mechanism (high dependency of wear on film thickness) will continue to erode the central part of the tooth until the load is carried on the outer thirds of its extent where the entrainment mechanism is more effective in generating oil films.

Figure 17 is a photograph of a worm wheel tooth showing two of the teeth taken from endurance testing carried out at Renold gears. The wheel is shown with the tips of the teeth pointing downwards with the throat area of each tooth in the foreground. The gears were subject to 1200 h of test running in an accelerated wear test at 180 per cent overload. The area of greatest wear is identified and can be seen to correspond qualitatively to that emerging from the calculations as shown in Fig. 12. The wear pattern is the same for both the teeth shown but it should be noted that the root portion of the lower tooth in the figure is hidden by the upper tooth.

A further comparison that can be made is with the results of the wear model developed by Egorov and

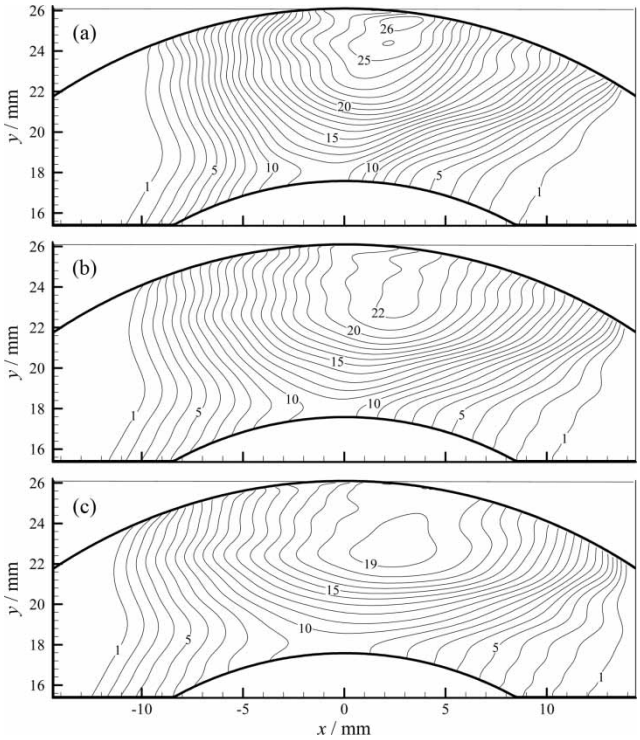

Fig. 12 Accumulated wear/μm when total material removed is 2.2 mm^3 with boundaries defined by relieving radius of 40 mm, (a) $n = 2.24$, (b) $n = 1$, (c) $n = 0$

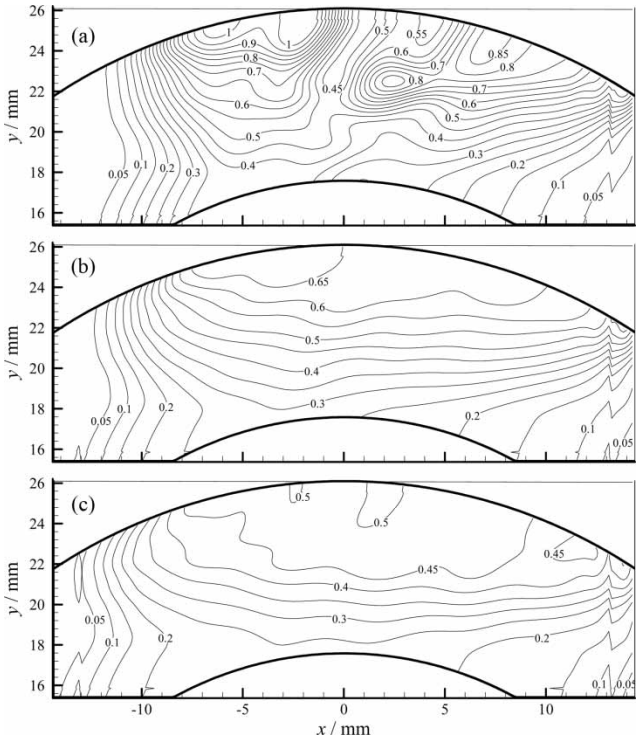

Fig. 13 Calculated wear rate/μm ΔT^{-1} when total material removed is 2.2 mm^3 with boundaries defined by relieving radius of 40 mm, (a) $n = 2.24$, (b) $n = 1$, (c) $n = 0$

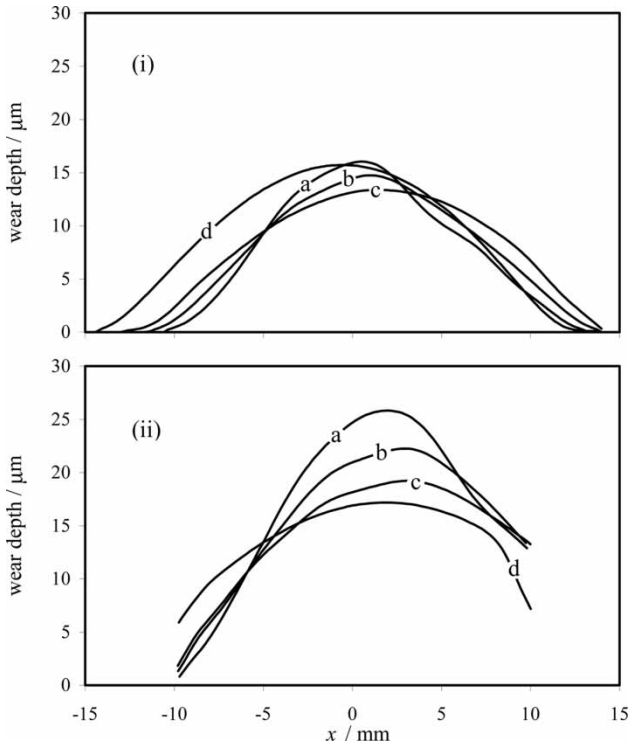

Fig. 14 Accumulated wear profiles at position (i) $y = 20$ mm and (ii) $y = 24$ mm in Fig. 12: (a) $n = 2.24$, (b) $n = 1$, (c) $n = 0$, (d) in Fig. 18

Morrish [**14**] as part of the same research project. The wear rate in this model is based on local pressure only and that pressure is calculated from simple cantilever stiffness calculations along the tooth. Its advantage is that it can run rapidly and incorporates dynamic evaluation of load share between simultaneously contacting pairs of teeth during the wear calculation. Figure 18 shows the result of the Egorov and Morrish model for the test case used in the current paper and is produced to correspond to the same degree of wear in terms of material removal, as is presented in Fig. 12. The appropriate comparison is with the result presented in Fig. 12(iii) for which the wear rate formula used in both approaches correspond. The results shown in contour form in Fig. 18 are also included in the wear profiles of Fig. 14 (curves d). Figure 18 shows closed contours at the outer worm radius whereas the contours in Fig. 12 remain open to the boundary. This difference and those in the profiles in Fig. 14 are due to the differences between the load share profiles adopted in the models. It is intended that the technique developed by Egorov and Morrish will be extended to incorporate a film thickness dependence in due course.

5 DISCUSSION AND CONCLUSIONS

A theoretical model of wear in worm gears has been developed. The treatment is based on an EHL analysis that reveals the detailed distribution of pressure and film thickness in the contact between the gear teeth, together with the use of a modified Archard-type wear law to calculate the rate of material removal under low lambda-ratio conditions. The pattern of predicted wear on the wheel tooth shows that the way in which film thickness is assumed to influence wear has a dominant effect on the amount of wear taking place. It is therefore suggested that to predict wear in practice it is necessary to determine the relation between wear rate and film thickness in simple wear experiments using the gear materials concerned.

In general, it is found that a high sensitivity of wear to film thickness has the effect of concentrating the wear at the middle part of the wheel tooth area. In

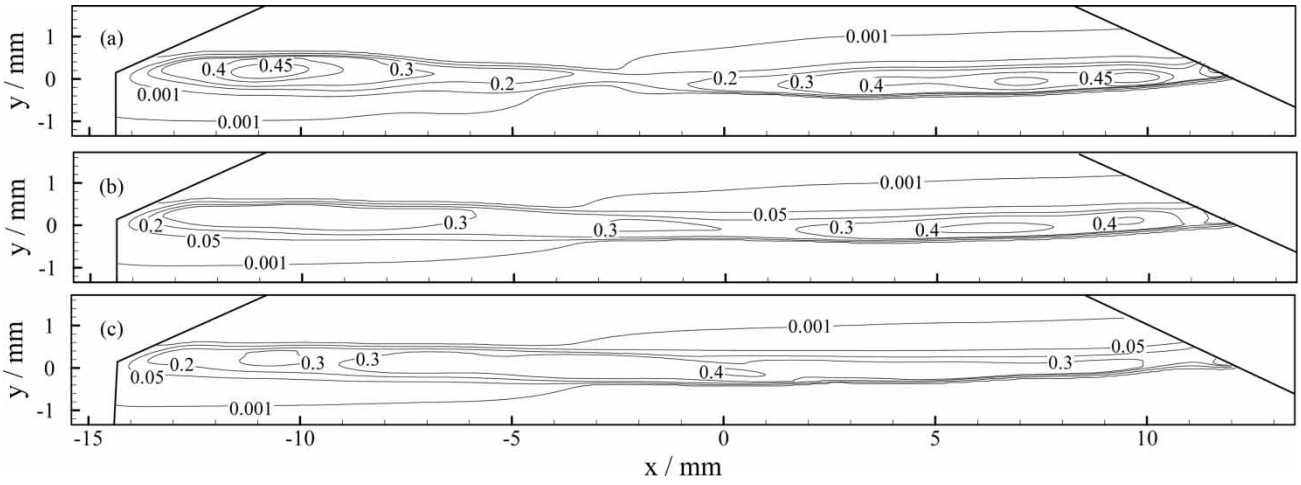

Fig. 15 Contours of pressure/GPa a particular mesh position when total material removed is 2.2 mm^3 (a) $n = 2.24$, (b) $n = 1$, (c) $n = 0$

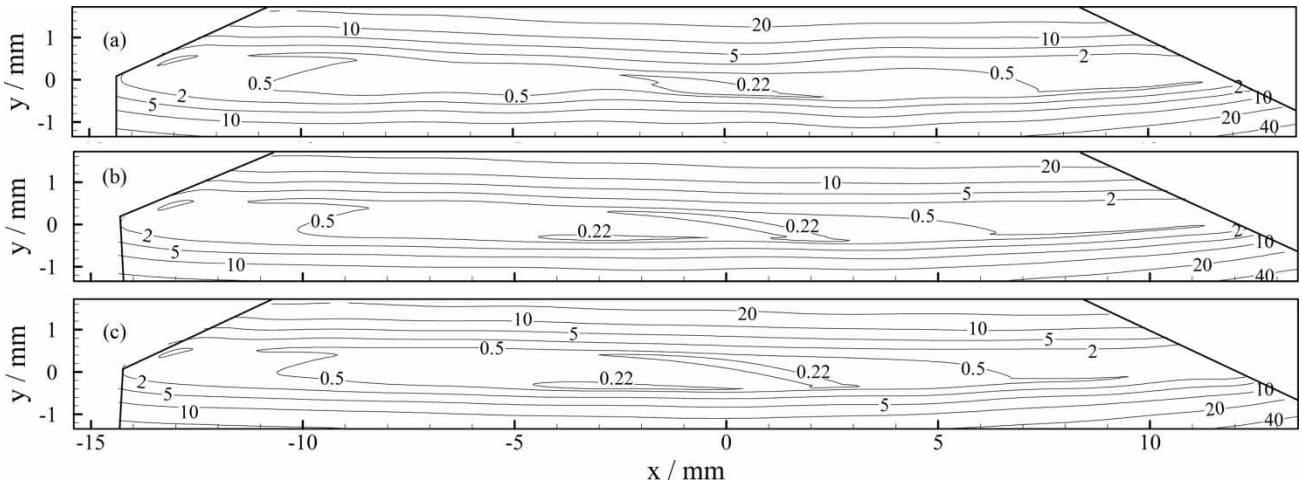

Fig. 16 Contours of film thickness/μm at a particular mesh position when total material removed is 2.2 mm^3 (a) $n = 2.24$, (b) $n = 1$, (c) $n = 0$

this region the contact is subject to severe film thinning due to poor hydrodynamic entrainment conditions. The modification of the tooth surface geometry brought about by wear does not necessarily relieve this situation, and poor film generation continues to characterize this part of the tooth surface. Wear continues in this area until sufficient material is removed to relieve the pressure locally and thereby reduce the rate of wear. This characteristic behaviour has the effect of effectively splitting the contact area into two separate load bearing regions, one on either side of a high-wear central band.

In less aggressive cases (i.e. smaller values of n) where thin films do not produce severe local behaviour the tendency is for the development of a more uniformly distributed wear pattern that leads to a sharing of load across the whole of the tooth. This effect is clearly demonstrated, for example, in Fig. 15 in which the EHL pressure is seen to be almost constant across the contact. It is not possible to disassociate the wear model from the changes that wear will produce in the load share pattern between successive teeth.

It is suggested that, when used in conjunction with data from simple wear experiments in which the influence of film thickness (or lambda ratio) on wear rate is determined, the model presented here and in reference [**12**] can be used as a practical aid for predicting wear in worm gears. The EHL modelling at the heart of the current study is necessarily time consuming and to obtain a rapid analysis and design tool there are clear advantages to developing

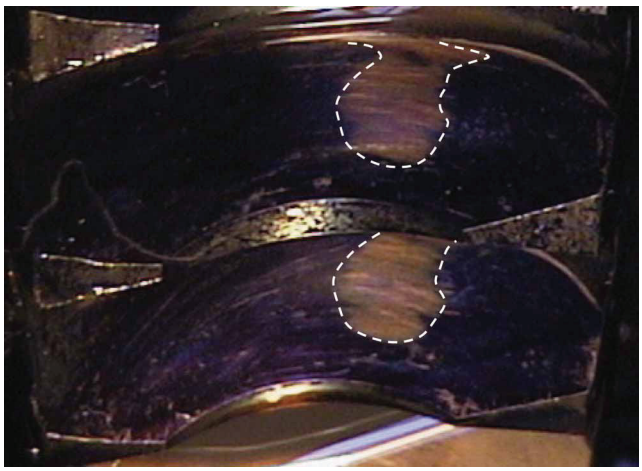

Fig. 17 Photograph of a worm wheel tooth from endurance testing carried out at Renold Gears. These gears had run for 1200 hours in an accelerated wear test at 180% overload. The area of greatest wear is identified and can be seen to correspond qualitatively to those emerging from the calculations as shown in Fig. 12. Note that the wear pattern is the same for both the teeth shown but that the root of the lower tooth in the figure is hidden by the upper tooth

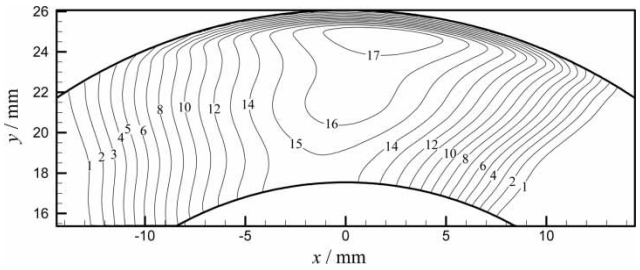

Fig. 18 Contours of wear/μm produced by tooth flexure load share model without any film thickness dependence [**14**] which is a comparable case to Fig. 12 (iii)

means of parameterizing its input to the wear calculation within the framework of the approach adopted in reference [**14**].

ACKNOWLEDGEMENTS

The authors gratefully acknowledge the support of EPSRC and MOD/DSTL for the research grant GR/R15429/01 that allowed this work to be carried out.

REFERENCES

1 **Sharif, K. J., Kong, S., Evans, H. P.,** and **Snidle, R. W.** Contact and elastohydrodynamic analysis of worm gears: Part 1 theoretical formulation. *Proc. Instn Mech. Engrs, Part C: J. Mechanical Engineering Science*, 2001, **215**, 817–830.

2 **Sharif, K. J., Kong, S., Evans, H. P.,** and **Snidle, R. W.** Contact and elastohydrodynamic analysis of worm gears: Part 2 results. *Proc. Instn Mech. Engrs, Part C: J. Mechanical Engineering Science*, 2001, **215**, 831–846.

3 **Fish, M. A.** and **Munro, R. G.** Modelling contact characteristics in worm gear systems. Br. Gear Association Technical Congress, 1999.

4 **Morris, S. J., Evans, H. P.,** and **Snidle, R. W.** Comparison of non-Newtonian EHL models in high sliding applications. In Proceedings of 27th Leeds-Lyon Symposium on *Tribology*, Lyon, 2000, pp. 787–796 (Elsevier, Amsterdam, 2001).

5 **Holmes, M. J. A., Evans, H. P., Hughes, T. G.,** and **Snidle, R. W.** Transient elastohydrodynamic point contact analysis using a new coupled differential deflection method: Part 1. Theory and validation. *Proc. Instn Mech. Engrs, Part J: J. Engineering Tribology*, 2003, **217**, 289–303.

6 **Archard, J. F.** Contact and rubbing of flat surfaces. *J. Appl. Phys.*, 1953, **24**, 981–988.

7 **Peterson, M. B.** and **Winer, W. O.** (Eds) *Wear control handbook*, 1980 (American Society of Mechanical Engineers, New York).

8 **Medina, S.** and **Olver, A. V.** An analysis of misaligned spline couplings. *Proc. Instn Mech. Engrs, Part J: J. Engineering Tribology*, 2002, **216**, 269–279.

9 **Hohn, B.-R.** and **Streingrover, K.** *DIN 3996: a new standard for calculating the load capacity of worm gears*. AGMA Technical Paper 98FTM10, 1998.

10 **Fish, M. A.** and **Munro, R. G.** Isolating and quantifying tooth deformation in worm gear systems operating under a torque load. Lamdamap Conference, Longhirst Hall, Northumberland, July 1999.

11 **Sudoh, K., Tanaka, Y., Matsumoto, S.,** and **Tozaki, Y.** Load distribution analysis method for cylindrical worm gear teeth. *JSME Int. J., Series C*, 1996, **39**, 606–613.

12 **Sharif, K. J., Evans, H. P.,** and **Snidle, R. W.** Prediction of the wear pattern in worm gears. *Wear*, in press.

13 **Holmes, M. J. A., Evans, H. P.,** and **Snidle, R. W.** Analysis of mixed lubrication effects in simulated gear tooth contacts. *Trans. ASME J. Tribol.*, 2005, **217**, 61–69.

14 **Egorov, I. M.,** and **Morrish, L.** Wear modelling of worm gears. Private communication – to be submitted to *Proc. Instn Mech. Engrs, Part J: J. Engineering Tribology*.

APPENDIX

Notation

C, D	flow parameters in Reynolds equation (ms)
f	pressure influence coefficient in differential deflection equation (m^{-1})
h	lubricant film thickness (m)
H	wheel tooth hardness (Pa)
K	wear coefficient
n	film thickness parameter in wear formula
p	lubricant pressure (Pa)
R_a	roughness average (m)
u_s	sliding velocity i.e. relative velocity of surfaces (ms^{-1})
$\hat{U}$, $\hat{V}$	entrainment velocity in x- and y-axis directions (ms^{-1})
W	load (N)
β	angle between sliding direction and x-axis
δ	depth of material removed during one meshing cycle (m)
ΔT	wear step over which wear rate is assumed unchanged (s)
Δw	maximum depth of material removed during wear step ΔT (m)
ϕ	gap between undeformed surfaces (m)